Partial oxidation of propane to synthesis gas over noble metals-promoted Ni/Mg(Al)O catalysts -High activity of Ru-Ni/Mg(Al)O catalyst-

Masato Shiraga,[1] Dalin Li,[1] Ikuo Atake,[1] Tetsuya Shishido,[2] Yasunori Oumi,[1] Tsuneji Sano[1] and Katsuomi Takehira[1]*

[1]*Department of Chemistry and Chemical Engineering, Graduate School of Engineering, Hiroshima University, Kagamiyama 1-4-1, Higashi-Hiroshima 739-8527, Japan*
[2]*Department of Molecular Engineering, Graduate School of Engineering, Kyoto University, Katsura 1, Nishigyo-ku, Kyoto 615-8510, Japan*

Received 2006

*Correspondence should be addressed to:

Professor Katsuomi Takehira
Department of Chemistry and Chemical Engineering,
Graduate School of Engineering, Hiroshima University,
Kagamiyama 1-4-1, Higashi-Hiroshima, 739-8527, Japan
Phone : (+81-824)-24-6488
Telefax: (+81-824)-24-6488
E-mail: takehira@hiroshima-u.ac.jp

Abstract

Effect of the addition of small amount of noble metal, *i.e*. Ru, Rh, Pd, Ir or Pt, in the Ni/Mg(Al)O catalyst on the catalytic activity for the partial oxidation of propane has been investigated. $Mg_{2.5}(Ni_{0.5})$-Al hydrotalcite was prepared by co-precipitation and was calcined to form $Mg_{2.5}(Al,Ni_{0.5})O$ periclase. When the powders of the periclase were dipped in an aqueous solution of the nitrate of Ru(III), Rh(III), Pd(II), Ir(III) or Pt(II), a reconstitution of the hydrotaclite took place on the surface of $Mg_{2.5}(Al,Ni_{0.5})O$ particles due to a "memory effect." The calcination followed by the reduction of the dipped samples produced highly dispersed noble metal-Ni supported catalysts. The loading of noble metal gave rise to a decrease in the reduction temperature of Ni^{2+} to Ni^0 on $Mg_{2.5}(Al,Ni_{0.5})O$ periclase, an increase in the amount of H_2 uptake on the Ni metal and moreover a decrease in the particle size of Ni metal formed on the noble metals-Ni/$Mg_{2.5}$(Al)O catalyst. When the noble metals-$Ni_{0.5}/Mg_{2.5}$(Al)O catalysts were tested in the temperature-cycled operation of propane partial oxidation between 400 ºC and 700 ºC, the deactivation due to both Ni oxidation and coke formation on the catalyst was effectively suppressed by the loading of noble metals. The combination of Ru and $Ni_{0.5}/Mg_{2.5}$(Al)O was the most effective; the high sustainability against both Ni oxidation and coke formation was obtained only with 0.1 wt% of Ru loading. A dipping of 1.0 g of the powders of $Ni_{0.5}/Mg_{2.5}$(Al)O periclase in a 5 ml of Ru(III) nitrate-aqueous solution was enough to reconstitute the hydrotalcite on the surface of the powder particles, leading to the formation of the Ru-Ni bimetal loaded catalyst with the high activity as well as the high sustainability.

Key Words: propane partial oxidation, H_2 production, Ru-Ni/Mg(Al)O catalyst, memory effect, hydrotalcite.

1. Introduction

Hydrogen is important in oil refineries and the chemical industry, and it is becoming attractive as a future clean fuel for combustion engines and fuel cells [1,2]. Steam reforming of hydrocarbons, especially of CH_4, has been employed frequently as the largest and generally the most economical way to make H_2 [3]. Endothermic steam reforming is the most hydrogen-efficient process and still remains as the main process for the production of hydrogen [1-3]. This process has been well established and optimized over the decades. Most often nickel catalysts, which combine low costs and high activity, are used [3]. Despite all this, the steam reforming process faces several drawbacks; the most significant one being the large energy input needed for the reaction. Therefore, hydrogen production by the non-catalytic partial oxidation of hydrocarbons has become the second most important process. Its main advantage is that it is exothermic, but the reaction requires very high temperature [1,2]. Consequently, the catalytic partial oxidation has received considerable attention over the past years. Research concerning the catalytic partial oxidation has been focused on CH_4, as it is believed to be still a future major feedstock for the production of hydrogen.

We have reported that Ni/Mg(Al)O catalyst derived from hydrotalcite(HT)-like compounds produced highly dispersed and stable Ni metal particles on the surface

[4-10] and were successfully applied in the steam reforming and oxidative reforming of CH_4 [6,7]. However, the Ni/Mg(Al)O catalysts were quickly deactivated due to the oxidation of Ni metal not only by oxygen gas but also by steam when they were applied in the daily startup and shutdown (DSS) operation of steam reforming of CH_4 [11]. The combination of small amount of noble metals and Ni/Mg(Al)O catalysts has been found to be effective for suppressing the Ni oxidation during the DSS operation [12,13]. In the steady state reaction, a similar approach has been tried in the preparation of Rh-Ni/Mg(Al)O catalyst in the partial oxidation or the oxidative steam reforming of CH_4 [14,15] and noble metals-Ni/Mg(Al)O catalysts in the dry reforming of CH_4 [9]. The behaviors of Ni/MgO catalyst were improved by the addition of noble metals; Rh, Pt and Pd were successfully incorporated in the Ni/MgO catalyst for the steady state oxidative steam reforming of CH_4 [16-18]. The addition of Pt, Ir and Ru on the Ni/γ-Al_2O_3 or Ni/$MgAl_2O_4$ catalyst resulted in an increase in metal surface area and moreover the catalysts obtained were self-activated in the reforming reaction without pre-reduction [19-21].

In contrast to CH_4, only introductory studies concerning the partial oxidation of higher hydrocarbons have been limited to noble metal catalysts [22-26]. The extensive work by Schmidt and co-workers on short contact-time reactors [22,23] showed that Rh has high activity and selectivity, superior to that of other noble metals. Rh-impregnated alumina foams and metallic microchannel reactors were studied for production of hydrogen-rich syngas through short contact-time catalytic partial oxidation of propane [25,26]. However, these noble metal loaded catalysts do not seem acceptable for this process due to their high cost.

Only a few papers have been reported on nickel loaded catalysts for the partial oxidation of higher hydrocarbons [27,28]. Nickel supported catalysts were modified by alkali metal or rare-earth metal oxides [27]. Ni/Mg(Al)O catalysts were prepared from HT as the precursors [28]. As a bimetallic catalyst, Pt-Ni/δ-Al_2O_3 was successfully devoted to the oxidative reforming of propane and butane [29-31]. The bimetallic systems showed superior catalytic performances compared to the monometallic systems probably due to the actions as micro heat exchangers; the heat generated by Pt sites during the exothermic total oxidation being readily transferred through the catalyst particles acting as micro heat exchangers to the Ni sites, which promote endothermic steam reforming.

Further extensive studies have to be looked forward to develop inexpensive and sustainable catalyst for the production of hydrogen as a future clean fuel. In this contribution, we report an improved behavior of Ru, Rh, Pd, Ir and Pt-$Ni_{0.5}$/$Mg_{2.5}$(Al)O bimetallic catalysts in the partial oxidation of propane under accelerated deactivation conditions.

2. Experimental

2.1. Catalyst preparation

Ni loaded Mg(Al)O catalyst with the Mg/Ni/Al composition of 2.5/0.5/1 was prepared by co-precipitation following the previous works [4-10]; $Mg_{2.5}(Ni_{0.5})$-Al HT-like precursor, in which a part of Mg^{2+} in Mg-Al HT was replaced by Ni^{2+}, was prepared by co-precipitation of the nitrates of the metal components. An aqueous

solution containing the nitrates of Mg^{2+}, Ni^{2+} and Al^{3+} was added slowly into an aqueous solution of sodium carbonate. Simultaneously pH of the solution was adjusted at 10 by adding an aqueous solution of sodium hydroxide with vigorous stirring. During the mixing treatment, heavy slurry precipitated. The crystal growth took place by aging the solution at 90 ºC for 12 h. After the solution was cooled to room temperature, the precipitate was washed with de-ionized water and dried in air at 100 ºC. The $Mg_{2.5}(Ni_{0.5})$-Al HT-like precursor was calcined in a muffle furnace in a static air atmosphere by increasing the temperature from ambient temperature to 650 ºC at a rate of 5 ºC min^{-1} and kept at 650 ºC for 14 h, followed by calcination at 900 ºC for 5 h, to form $Mg_{2.5}(Al,Ni_{0.5})O$ periclase as the precursor of $Ni_{0.5}/Mg_{2.5}(Al)O$ catalysts. Ni loading was 13.5 wt% by ICP analyses after the calcinination at 900 ºC. As a control, $Mg_3(Al)O$ periclase was prepared by calcining Mg_3-Al HT obtained by co-precipitation; the co-precipitation followed by the calcination was carried out in a similar procedure as above.

Loadings of noble metals, Ru, Rh, Pd, Ir and Pt, have been done by adopting a "memory effect" of Mg(Ni)-Al HT [12]; 1.0 g of the powders of $Mg_{2.5}(Al,Ni_{0.5})O$ periclase were dipped in an aqueous solution of the nitrate of Ru(III), Rh(III), Pd(II), Ir(III) or Pt(II) for 1 h at room temperature, followed by drying in air at 100 ºC. A prescribed amount of the nitrate of each noble metal depending on the loading amount was dissolved in 5 ml of de-ionized water if not specifically mentioned. During the dipping followed by the drying treatments, $Mg_{2.5}(Ni_{0.5})$-Al HT was reconstituted from $Mg_{2.5}(Al,Ni_{0.5})O$ periclase due to the "memory effect." During the reconstitution, noble metal was incorporated either by replacing the Mg^{2+} or the Al^{3+} site or by physically

trapped in the layered structure of the HT. The sample was finally calcined at 850 ºC for 5 h to form the precursor of Ru, Rh, Pd, Ir or Pt-$Ni_{0.5}/Mg_{2.5}$(Al)O catalysts. The powders of the precursors were pressed to a disc, crushed roughly and sieved to the particles of 0.36-0.60 mmΦ, and used in the reforming reactions. As a control, 0.1 wt%Ru/Mg_3(Al)O was prepared using Mg_3(Al)O periclase as the catalyst support in a similar way.

Also as a control, *iw*-13.5 wt% Ni/γ-Al_2O_3 catalyst was prepared by incipient wetness method using γ-Al_2O_3 and an aqueous solution of Ni(II) nitrate. Commercial Ni and Ru catalysts were supplied from Süd-Chemie Catalysts Japan, Inc. and were also used as controls. FCR (12 wt%Ni/α-Al_2O_3) and RUA (2 wt%Ru/α-Al_2O_3) as received were first crushed to fine powders, pressed to a disc, crushed roughly, sieved to the particles of 0.36-0.60 mmΦ and used in the reforming reactions. BET surface area was 7.0 and 6.5 $m^2\ g_{cat}^{-1}$ for FCR and RUA as the particles, respectively.

2.2. Characterization of catalyst

The structure of the catalysts was studied by using XRD, TEM, TPR, TPO, TG-DTA, ICP, N_2 and H_2 adsorption method.

Powder X-ray diffraction was recorded on a Mac Science MX18XHF-SRA powder diffraction-meter with mono-chromatized Cu Kα radiation (λ = 0.154 nm) at 40 kV and 200 mA. The diffraction pattern was identified by comparing with those included in the JCPDS (Joint Committee of Powder Diffraction Standards) data base. A particle size of Ni metal on the catalyst was calculated from Scherrer equation: $d = K\lambda/\beta\cos\theta$; β, full width at half maximum; $K = 0.94$ and $\lambda = 1.5405$ Å.

Transmission electron micrographs (TEM) were obtained over a JEOL JEM3000F instrument equipped with a Hitachi/Kevex H-1800/DeltaIV EDS for monitoring the carbon fibers formed on the catalysts.

Temperature-programmed reduction (TPR) of the catalyst was performed at a heating rate of 10 ºC min^{-1} using a H_2/Ar (5/95 ml min^{-1}) mixed gas as reducing gas after passing through a 13X molecular sieve trap to remove water. A U-shaped quartz tube reactor (6 mm i.d.) equipped with a TCD for monitoring the H_2 consumption was used. Prior to the TPR measurements, the sample was calcined at 300 ºC for 2 h in an O_2/Ar (10/40 ml min^{-1}) mixed gas.

A temperature programmed oxidation (TPO) experiment was performed on the catalyst after the reaction from room temperature to 900 ºC at a heating rate of 2.5 ºC min^{-1} in an O_2/N_2 (5/20 ml min^{-1}) mixed gas. The amount of coke formed on the catalyst was estimated from the amount of CO_2 formed during the TPO experiment.

Temperature gravimetric and differential thermal analysis (TG-DTA) curve was recorded under an inert atmosphere of N_2 (20 ml min^{-1}) with Shimadzu TG-DTA-50 analyzers using 50 mg of sample and at a heating rate of 10 ºC min^{-1}.

Inductively coupled plasma spectroscopy (ICP) measurement was carried out on a Perkin-Elmer OPTIMA 3000 spectrometer. The content of each metal component was determined after the sample was completely dissolved using diluted hydrochloric acid and a small amount of hydrofluoric acid.

The N_2 adsorption (-196 ºC) study was used to examine the BET surface area of the catalyst. The measurement was carried out on a Shimadzu Micromeritics Flowsorb 2300, and all samples (ca. 100 mg) were pretreated in a N_2/H_2 (50/50 ml min^{-1}) mixed

gas at 300 ºC for 1 h before the measurements.

Ni dispersion was determined by static equilibrium adsorption of H_2 at ambient temperature using the pulse method. A 50 mg portion of the catalyst was reduced at 900 ºC in a mixed gas flow of 20 vol.% H_2/N_2 (25 ml min^{-1}) for 1 h; this reduced catalyst was used for the measurement. During the pulse experiment, the amount of H_2 was monitored by a TCD-gas chromatograph. Uptake of H_2 at monolayer coverage of the Ni species was used to estimate Ni metal dispersion and particle size. Thus the equation used to calculate dispersion was:

$$\%D = 1.17X / Wf \quad (1)$$

where X = H_2 uptake in μmoles / g of catalyst, W = the weight percent of nickel, and f = the fraction of nickel reduced to the metal. f was assumed as 80 % and 100 % for hydrotalcite derived catalysts [13] and impregnated catalyst, respectively. Average crystallite diameters were calculated from %D assuming spherical metal crystallites, all having the same size d [32]:

$$d = 971 / (\%D) \quad (2)$$

2.3. Kinetic measurements

Partial oxidation of propane was conducted using a fixed bed-flow reactor in a $C_3H_8/O_2/N_2$ (10.0/18.7/71.3 ml min^{-1}) mixed gas over 50 mg of the catalyst with a temperature-cycled reaction mode (Fig. 1). The catalyst was used as the particles of 0.36-0.60 mmΦ dispersed in 50 mg of quartz sand. A U-shaped quartz tube reactor (6 mm i.d.) was used, with the catalyst bed near the bottom. N_2 was used as an internal standard for calculating the C_3H_8 conversion and the yields of products. After

pre-reduction of the catalyst in a H_2/N_2 (5/25 ml min^{-1}) mixed gas at 900 ºC for 60 min, the reaction was started at 700 ºC. After starting the reaction, the reaction temperature was decreased from 700 ºC to 400 ºC stepwise by every 100 ºC, and then increased at once from 400 ºC to 600 ºC again, during which the activity was tested for 90 min at each reaction temperature. Throughout these temperature variations, the $C_3H_8/O_2/N_2$ (10.0/18.7/71.3 ml min^{-1}) mixed gas was continuously flowed through the reactor. At low temperature, the combustion reaction takes precedence over the reforming reactions. As a result, the reaction atmosphere becomes thermodynamically oxidative, where the deactivation of the Ni catalysts might be accelerated by the oxidation of Ni metal. Thus the accelerated deactivation test was carried out for each catalyst using the temperature-cycled mode. The thermocouple to control the reaction temperature was placed at the center of the catalyst bed. Product gases were analyzed by online TCD-gas chromatography.

3. Results

3.1. Reconstitution of HT.

Typical XRD patterns of the samples during the preparation of the 0.1 wt%Ru-$Ni_{0.5}/Mg_{2.5}$(Al)O catalyst are shown in Fig. 2. The reflection lines of $Mg_{2.5}(Ni_{0.5})$-Al HT were observed for the sample as deposited by co-precipitation (Fig. 2a) and those of $Mg_{2.5}(Al,Ni_{0.5})O$ periclase appeared after the calcination at 900 ºC (Fig. 2b). After dipping the powders of $Mg_{2.5}(Al,Ni_{0.5})O$ periclase in 5 ml of an aqueous solution of Ru(III) nitrate for 1 h followed by the drying in air at 100 ºC, Mg(Ni)-Al HT

was reconstituted although the line intensity was weak (Fig. 2c). During the dipping treatment, the reconstitution of HT proceeded by the "memory effect." The HT reconstitution was actually limited to the surface layer of the particles due to a use of the small amount of aqueous solution, since the lines of $Mg_{2.5}(Al,Ni_{0.5})O$ periclase still remained intensively. A similar phenomenon was reported previously in the preparation of eggshell-type Ni loaded Mg(Al)O catalysts [10]. It must be noticed that Ru(III) is not chemically incorporated but is physically trapped in the $Mg_{2.5}(Ni_{0.5})$-Al HT layer after the reconstitution (*vide infra*). When the HT-reconstituted sample was caclined at 900 ºC for 5 h, the lines of the HT disappeared and those of $Mg(Ni)Al_2O_4$ spinel weakly appeared together with those of $Mg_{2.5}(Al,Ni_{0.5})O$ periclase as main phase (Fig. 2d). The formation of spinel is probably due to the repeated heating treatments at 900 ºC before and after the dipping treatment. The lines of Ni metal appeared after the reduction of the calcined sample at 900 ºC for 1 h (Fig. 2e).

The other noble metals-Ni bimetal catalysts showed a similar change in the XRD patterns during the preparation; the HT was reconstituted due to the "memory effect" after dipping the powders of $Mg_{2.5}(Al,Ni_{0.5})O$ periclase in all aqueous solutions of the nitrates of Rh(III), Pd(II), Ir(III) and Pt(II).

3.2. Sustainability of the Ni catalysts.

The results of temperature-cycled operation of the partial oxidation of propane over the supported Ru, Rh, Pd, Ir and Pt catalysts are shown in Fig. 3 together with those over the $Ni_{0.5}/Mg_{2.5}(Al)O$, *imp*-Ni/γ-Al_2O_3, RUA and FCR catalysts as controls. The conversion of propane decreased with decreasing the reaction temperature from

700 ºC to 400 ºC and again recovered, i.e., increased, with increasing the temperature to 600 ºC; both decrease and recovery of the activity clearly depended on the metal species and the preparation method of the catalysts (Fig. 3A). The activities of both $Ni_{0.5}/Mg_{2.5}(Al)O$ and *imp*-Ni/γ-Al_2O_3 significantly decreased at 400 ºC and their recoveries in the activity at 600 ºC were small. Among the commercial catalysts, FCR showed a low activity together with a severe deactivation at 400 ºC, and moreover the worst activity recovery at 600 ºC. On the other hand, RUA showed a considerable deactivation with decreasing the temperature from 700 ºC to 400 ºC, while a good recovery in the activity at 600 ºC was observed. Among the noble metals-Ni bimetallic catalysts, the highest sustainability and the highest recovery were obtained over the Ru- and Rh-$Ni_{0.5}/Mg_{2.5}(Al)O$ catalysts, followed by the Pd-, Pt- and Ir-$Ni_{0.5}/Mg_{2.5}(Al)O$ catalysts. The rate of H_2 production was 4.3 mol h^{-1} g_{cat}^{-1} for the Ru-$Ni_{0.5}/Mg_{2.5}(Al)O$ catalysts at 700 ºC.

The results of temperature-cycled operation over the Ru-$Ni_{0.5}/Mg_{2.5}(Al)O$ catalysts with varying Ru loadings are shown in Fig. 4. The catalytic behavior of $Ni_{0.5}/Mg_{2.5}(Al)O$ was improved by the Ru loading; propane conversion at 400 ºC increased with increasing Ru loading up to 0.1 wt%, indicating increasing sustainability of the catalyst. However 0.5 wt% Ru loading caused a sudden decrease in the sustainability; this is due to the phase separation of RuO_2 from Ni-Ru bimetallic system as seen in the data of TPR (*vide infra*).

In the absence of Ru, the $Ni_{0.5}/Mg_{2.5}(Al)O$ catalyst showed a transient phenomenon at the beginning of the 2nd reaction at 600 ºC; both C_3H_8 conversion and rate of H_2 formation (data are not shown) decreased and simultaneously H_2O selectivity

increased up to 80 % (Figs. 3B). This is probably due to a transient reduction of Ni species, indicating that the oxidized Ni surface was gradually reduced under the reaction conditions at 600 ºC. Such transient phenomenon disappeared by the loading of noble metals on the $Ni_{0.5}/Mg_{2.5}(Al)O$ catalyst, resulting in a good recovery in the activity at 600 ºC. It is concluded that the combination with noble metals donates the sustainability on the $Ni_{0.5}/Mg_{2.5}(Al)O$ catalyst during the temperature-cycled operation of propane partial oxidation.

..

3.3. Deactivation of the Ni catalysts.

Partial oxidation of propane over Ni catalysts proceeds *via* combustion (3), followed by steam and dry reforming reactions (4 and 5). Direct partial oxidation of

$$C_3H_8 + 5O_2 \rightarrow 3CO_2 + 4H_2O \qquad \Delta H^0_{298} = -2046 \text{ kJ mol}^{-1} \quad (3)$$

$$C_3H_8 + 3H_2O \rightarrow 3CO + 7H_2 \qquad \Delta H^0_{298} = +497 \text{ kJ mol}^{-1} \quad (4)$$

$$C_3H_8 + 3CO_2 \rightarrow 6CO + 4H_2 \qquad \Delta H^0_{298} = +620 \text{ kJ mol}^{-1} \quad (5)$$

propane (6) can proceed on Rh-supported catalysts as reported with short contact-time

$$C_3H_8 + 3/2O_2 \rightarrow 3CO + 4H_2 \qquad \Delta H^0_{298} = -229 \text{ kJ mol}^{-1} \quad (6)$$

reactors [19,20], and an excess loading of Ru on the $Ni_{0.5}/Mg_{2.5}(Al)O$ catalyst resulted in an appearance of such activity (*vide infra*). However this contribution is minor on the present Ni metal catalysts. Water-gas shift reaction (7), methanation (8),

$$CO + H_2O \rightarrow CO_2 + H_2 \qquad \Delta H^0_{298} = -41 \text{ kJ mol}^{-1} \quad (7)$$

$$CO + 3H_2 \rightarrow CH_4 + H_2O \qquad \Delta H^0_{298} = -205 \text{ kJ mol}^{-1} \quad (8)$$

dehydrogenation of propane (9) and coke formation from propane (10) will play a role,

$$C_3H_8 \rightarrow C_3H_6 + H_2 \qquad \Delta H^0_{298} = +124 \text{ kJ mol}^{-1} \quad (9)$$

$$C_3H_8 \rightarrow 3C + 4H_2 \qquad \Delta H^0_{298} = +104 \text{ kJ mol}^{-1} \quad (10)$$

depending on reactant composition, temperature and heat transfer rate, residence time and the catalytic system involved. Additional side reactions, including cracking of propane (11) and carbon monoxide to carbon deposition (12) must be considered; the

$$C_3H_8 \rightarrow C_2H_4 + CH_4 \qquad \Delta H^0_{298} = +89 \text{ kJ mol}^{-1} \quad (11)$$

$$2CO \rightarrow C_{(s)} + CO_2 \qquad \Delta H^0_{298} = -172 \text{ kJ mol}^{-1} \quad (12)$$

latter is particularly unwonted and generally occurs when the O_2/C_3H_8 ratio in the reaction mixture becomes too low.

In the present work, the excess O_2/C_3H_8 molar ratio of 1.88 was adopted for accelerating deactivation compared with the molar ratio of 1.5 required for completing the syngas production by summing the reactions (3), (4) and (5). The selectivity to H_2O inversely well correlated to the decrease in propane conversion in both Fig. 3 and Fig. 4, suggesting that the deactivation takes place by the oxidation of Ni metal, resulting in an occurring of the combustion reaction (3). If the combustion reaction alone proceeded under the present reaction conditions, the conversion of propane would be 37.5 % taking account of the molar ratio 1.88 of O_2/C_3H_8 in the reaction (3). The $Ni_{0.5}/Mg_{2.5}(Al)O$ catalyst was severely deactivated at 400 ºC not only by the oxidation of Ni metal but also by the coking, etc., judging from the propane conversion of 33 % below 37.5 % (Fig. 3A). FCR showed only 0.6 % propane conversion and negligible small H_2 production at 400 ºC (Fig. 3A); this is certainly due to both severe Ni oxidation and heavy coking (*vide infra*), resulting in a damaging of the active sites not only for the reforming but also for the combustion. Interestingly, the activity was restored even after such heavy deactivation by increasing the reaction temperature to

600 ºC, suggesting that the oxidized Ni was re-reduced and the coke was removed by the combustion. The propane conversion was recovered to 40 % from 0.6 % even for the FCR catalyst (Fig. 3A); it is most likely that the coke was removed and the oxidized Ni was re-reduced since the rate of H_2 production was recovered up to 0.3 mol h^{-1} g_{cat}^{-1}, almost 50 % of that at the 1st step reaction at 600 ºC.

3.4. Properties of Ni-Ru bimetallic species.

Product distributions in the first step reaction at 700 ºC and coke deposition after the total temperature-cycled operation of the propane oxidation are shown in Table 1. Over both $Ni_{0.5}/Mg_{2.5}(Al)O$ and *iw*-13.5 wt%Ni/γ-Al_2O_3 catalysts, a small amount of C_2~C_3 compounds, i.e., C_2H_4, C_2H_6 and C_3H_6, were produced together with H_2, CO and CO_2 as the main products. It must be emphasized that significant coke formation occurred on these supported Ni catalysts. Over both 0.1 wt%Ru/Mg_3(Al)O and RUA catalysts, increased selectivity to C_2~C_3 compounds was observed together with that to CH_4, suggesting that Ru catalyzed the cracking of propane (11), but coking was not significant. The 0.1 wt% loading of noble metals on $Ni_{0.5}/Mg_{2.5}(Al)O$ remarkably suppressed both coking and formations of C_2~C_3 compounds except the case of Ir loading; the effect was the most evident by the Ru loading as observed on the 0.1 wt%Ru-$Ni_{0.5}/Mg_{2.5}(Al)O$ catalyst. Such properties of Ru-loaded catalysts among the 0.1 wt% noble metals-loaded $Ni_{0.5}/Mg_{2.5}(Al)O$ catalysts suggest that a remarkable synergy due to a strong interaction or a formation of alloy took place between Ru and Ni (*vide infra*).

Properties of the supported Ru, Rh, Pd, Ir and Pt catalysts, i.e., BET surface areas, H_2 uptakes, metal dispersion and particle sizes of Ni metal, are shown in Table 1. The surface area of $Ni_{0.5}/Mg_{2.5}(Al)O$ significantly decreased by the loading of noble metals. Also 0.1 wt%Ru loading on $Mg_3(Al)O$ itself resulted in a decrease in the surface area compared to the original value of 145.0 m^2 g_{cat}^{-1} of $Mg_3(Al)O$. Contrarily, H_2 uptake was drastically enhanced by the loading of noble metals on the $Ni_{0.5}/Mg_{2.5}(Al)O$ catalyst; H_2 uptake increased even with 0.01 wt% of Ru loading. At 0.1 wt% of noble metal loading, the Ru-, Rh- and Ir-$Ni_{0.5}/Mg_{2.5}(Al)O$ catalysts showed higher values of the H_2 uptake than the Pd- and Pt-$Ni_{0.5}/Mg_{2.5}(Al)O$ catalysts. The contribution of noble metal itself to the H_2 uptake on the noble metal-supported $Ni_{0.5}/Mg_{2.5}(Al)O$ catalysts must be small, since the 0.1 wt%$Ru/Mg_3(Al)O$ catalyst showed an extremely small value of the H_2 uptake. A synergetic effect between noble metals and Ni metal is likely to occur on the catalysts, leading to an enhancement in the H_2 uptake due to the bimetallic system formation such as alloy formation, etc.

4. Discussion

Deactivations of Ni-loaded catalysts caused by coking, sintering or oxidation of active metal species have been frequently reported [33-36]. Ni metal can be oxidized not only by gaseous oxygen but also even in the presence of steam as reported for lanthanide-promoted sol-gel Ni/Al_2O_3 catalyst in propane steam reforming [36] and for $Ni_{0.5}/Mg_{2.5}(Al)O$ catalyst in DSS-like steam reforming of methane [11]. Similar

deactivation by sintering or metal oxidation has been also seen in aqueous-phase reforming of oxygenated hydrocarbons over Raney Ni type catalysts at 250 ºC [37,38].

4.1. Coking on the catalysts.

Temperature programmed oxidation (TPO) was carried out for the catalyst after the reaction (Fig. 5). The 0.1 wt%Ru/Mg_3(Al)O catalyst showed no remarkable peak of CO_2 formation (Fig. 5a), whereas the $Ni_{0.5}$/$Mg_{2.5}$(Al)O catalyst showed clearly a peak of the CO_2 formation around 550 ºC (Fig. 5b). Coke formation was rather accelerated by 0.01 wt%Ru loading on the $Ni_{0.5}$/$Mg_{2.5}$(Al)O catalyst as observed as an intensive peak of the CO_2 formation around 530 ºC (Fig. 5c). This may be due to an enhanced propane conversion due to increasing catalytic activity. Further increase in the Ru loading led to a decrease in the coking and simultaneously to an increase in the peak temperature (Fig. 5d-f). Judging from the peak temperature in the TPO and the TEM observation (data are not shown), the coke materials belong to graphitic carbon in a form of carbon fibers on the catalysts. Considering the data of coking on various catalysts (Table 1), the carbon fibers are likely produced on the Ni metal particles by forming coke precursors derived from hydrocarbons or CO. The amount of coke materials from propane was much larger than that from methane; methane produced coke below 5 wt% on the $Ni_{0.5}$/$Mg_{2.5}$(Al)O catalyst under the same reaction conditions. In propane reforming, the probability to form the coke precursors is much higher than methane since propane produced C_2 and C_3 ad-species by cracking or dehydrogenation which may easily polymerize into polyaromatic compounds [39].

Ni metal catalysts can easily induce coke deposition directly from hydrocarbon (10) and due to the disproportionation of CO (10) [40]. Moreover C_3H_8 tends to form a larger amount of coke than CH_4 in the reforming reaction [39]. In the absence of noble metals, the $Ni_{0.5}/Mg_{2.5}(Al)O$ catalyst revealed remarkable coking, and moreover both *iw*-13.5 wt%Ni/γ-Al_2O_3 and 0.01 wt%Ru-$Ni_{0.5}/Mg_{2.5}(Al)O$ catalysts also showed further increasing coking in the partial oxidation of C_3H_8 (Table 2). On the other hand, the 0.1 wt% loading of noble metals on the $Ni_{0.5}/Mg_{2.5}(Al)O$ catalyst resulted in noticeable decreases in the coking. Among the noble metals tested, Ru was the most effective for suppressing the coking; an increase from 0.01 wt% to 0.5 wt% of its loading caused a drastic decrease in the coking, as well as an increase in the H_2 selectivity, on the Ru-$Ni_{0.5}/Mg_{2.5}(Al)O$ catalysts (Table 1).

4.2. Oxidation of Ni metal on the catalyst.

We have reported that gaseous oxygen or steam as the purge gas totally damaged Ni/Mg(Al)O catalysts by oxidizing the Ni metal during the DSS-like operation of steam reforming of CH_4 between 200 and 700 ºC [11]. No reflection line of Ni metal was observed for the deactivated Ni/Mg(Al)O catalysts after the DSS-like operation. Also in the present work, Ni metal on the $Ni_{0.5}/Mg_{2.5}(Al)O$, *iw*-13.5 wt%Ni/γ-Al_2O_3 and FCR catalysts was possibly oxidized by gaseous oxygen or steam during the temperature-cycled operation (Figs. 3 and 4). However, the reflection lines of Ni metal were still observed for both $Ni_{0.5}/Mg_{2.5}(Al)O$ and *iw*-13.5 wt%Ni/γ-Al_2O_3 catalysts although weakly and, moreover, rather intensively for the noble metals-supported $Ni_{0.5}/Mg_{2.5}(Al)O$ catalysts after the temperature-cycled operations. This can be seen for

the 0.1 wt%Ru-$Ni_{0.5}/Mg_{2.5}$(Al)O catalyst after the reaction (Fig. 2f). The intensity of the Ni metal reflection almost correlated with that of the propane conversion in the 2nd (or final) step reaction at 600 ºC (Fig. 3). It is likely that Ni species on the noble metals-supported $Ni_{0.5}/Mg_{2.5}$(Al)O catalysts was oxidized during the operations at the low temperatures of 500 and 400 ºC, and was re-reduced in the reaction at the final step at 600 ºC.

The conversion of oxygen was always higher than that of propane even at low temperature; oxygen was consumed almost perfectly at 700 ºC over all catalysts including FCR. At 400 ºC, oxygen conversions were 61, 3.6, 99 and 99 % on the $Ni_{0.5}/Mg_{2.5}$(Al)O, FCR, *iw*-13.5 wt%Ni/γ-Al_2O_3 and RUA catalysts, whereas those on 0.1 wt%Ru, Rh, Pd, Ir and Pt-$Ni_{0.5}/Mg_{2.5}$(Al)O catalysts were 100, 100, 98, 88 and 95 %, respectively. It must be noticed that even noble metals-loaded catalysts, such as RUA, the 0.1 wt%Pt-, 0.1 wt%Ir- and 0.1 wt%Pd-$Ni_{0.5}/Mg_{2.5}$(Al)O catalysts, were clearly deactivated at 400 ºC (Fig. 3A), although the oxygen conversion was quite high at 400 ºC. No significant coking took place on these catalysts. These suggest that the Ni catalysts could be deactivated by the Ni oxidation even in the absence of gaseous oxygen. The selectivity to H_2O during the temperature-cycled oxidation of propane is shown in Fig. 3B. RUA showed obviously high selectivity to H_2O at 400 ºC, followed by the *iw*-13.5 wt%Ni/γ-Al_2O_3, 0.1 wt%Pt-$Ni_{0.5}/Mg_{2.5}$(Al)O, $Ni_{0.5}/Mg_{2.5}$(Al)O, FCR, 0.1 wt%Ir-$Ni_{0.5}/Mg_{2.5}$(Al)O, 0.1 wt%Pd-$Ni_{0.5}/Mg_{2.5}$(Al)O, 0.1 wt%Rh-$Ni_{0.5}/Mg_{2.5}$(Al)O and 0.1 wt%Ru-$Ni_{0.5}/Mg_{2.5}$(Al)O catalysts. The order of deactivation shown by propane conversion over the noble metals-$Ni_{0.5}/Mg_{2.5}$(Al)O catalysts apparently well correlated with that of the selectivity to H_2O over the catalysts (Fig. 3A and B). Such correlation

between the catalyst deactivation and the selectivity to H_2O was observed also for the Ru-$Ni_{0.5}/Mg_{2.5}$(Al)O catalysts with the varying Ru loadings (Fig. 4A and B); the $Ni_{0.5}/Mg_{2.5}$(Al)O catalyst was the most severely deactivated, followed by the 0.01 wt%Ru-, 0.05 wt%Ru- and 0.1 wt%Ru-$Ni_{0.5}/Mg_{2.5}$(Al)O catalysts (Fig. 4A). It is suggested that the catalyst deactivation due to the Ni oxidation took place not only by gaseous oxygen but also by steam. Although CO_2 was produced together with H_2O in the propane oxidation, the catalyst deactivation by CO_2 cannot be taken account in the present work, since the $Ni_{0.5}/Mg_{2.5}$(Al)O catalyst was not deactivated by CO_2 purging in the DSS operation [11].

4.3. Effect of the preparation method on the HT reconstitution.

The "memory effect" was observed on the surface of the particles of $Mg_{2.5}$(Al,$Ni_{0.5}$)O periclase when they were dipped in an aqueous solution of Ru(III) nitrate (Fig. 2). Eggshell-type metal loading was achieved by controlling the dipping procedure [10]. We tried to control the reconstitution of the HT on the surface of $Mg_{2.5}$(Al,$Ni_{0.5}$)O particles as follows: the powder of $Mg_{2.5}$(Al,$Ni_{0.5}$)O periclase was dipped in varying amounts of aqueous solution of Ru(III) nitrate. Ru loading was fixed at 0.1 wt%. The 0.1 wt%Ru-$Ni_{0.5}/Mg_{2.5}$(Al)O catalysts were thus prepared by changing the amount of aqueous solution of Ru(III) nitrate and the dipping time (Table 3). The volume of the aqueous solution and the dipping time are marked at the end of catalyst symbol, e.g., 0.1 wt%Ru-$Ni_{0.5}/Mg_{2.5}$(Al)O (5, 1) for 5 ml and 1 h. The 0.1 wt%Ru-$Ni_{0.5}/Mg_{2.5}$(Al)O (0.4, 1) catalyst alone was prepared by "incipient wetness" method since the pore volume of 1.0 g of $Ni_{0.5}/Mg_{2.5}$(Al)O was obtained as 0.4 ml by

the DH method, whereas the other 0.1 wt%Ru-$Ni_{0.5}$/$Mg_{2.5}$(Al)O catalysts were prepared by “dipping” method. All catalysts were finally dried at 105 °C for one night and calcined. The powders of the precursors were pressed to a disc, crushed roughly and sieved to the particles of 0.36-0.60 mmΦ, and used in the reforming reactions.

XRD patterns of the samples dipped in 0.4, 5 and 40 ml of the aqueous solutions for 1 h are shown in Fig. 6. When $Mg_{2.5}(Ni_{0.5})$-Al HT co-precipitated (Fig. 6a) was calcined, the reflection lines of $Mg_{2.5}(Al,Ni_{0.5})O$ periclase appeared (Fig. 6b). The 0.1 wt%Ru-$Ni_{0.5}$/$Mg_{2.5}$(Al)O (0.4, 1) prepared by incipient wetness method showed no reflection line of Mg(Ni)-Al HT (Fig. 6c), indicating that no detectable reconstitution took place. The reflection lines of the $Mg_{2.5}(Ni_{0.5})$-Al HT appeared after the dipping in 5 ml of the aqueous solution for 1 h (Fig. 6d) and were intensified with increasing the volume of the aqueous solution from 0.4 ml to 40 ml (Fig. 6e). In these XRD patterns, the lines of $Mg_{2.5}(Al,Ni_{0.5})O$ periclase were always observed together with those of the HT, suggesting that the reconstitution of the HT from the periclase was restricted in the surface layer of the particles and was not completed throughout the powder particles. When $Mg_{2.5}(Al,Ni_{0.5})O$ periclase was dipped in 40 ml of the aqueous solution for 12 h, the reflection lines of $Mg_{2.5}(Al,Ni_{0.5})O$ periclase totally disappeared, whereas those of Mg(Ni)-Al HT were intensified; the reconstitution was completed throughout whole powder particles (Fig. 6f). Simultaneously the reflection of $Mg(OH)_2$ brucite appeared. The formation of $Mg(OH)_2$ brucite suggests that the reconstitution of HT from the periclase proceeds by the hydration of MgO followed by the dissolution, since MgO is thermodynamically unstable compared with $Mg(OH)_2$ [41]. MgO reacts even with moisture in the air, especially at low coordination atomic site, to form $Mg(OH)_2$ brucite.

As a control, the powder of $Mg_{2.5}(Ni_{0.5})$-Al HT before the calcination was also dipped in 5 ml of the aqueous solution of Ru(III) nitrate, resulting in no change in the XRD (Fig. 6g). No clear shift was observed in the reflection lines of in the HT of all the samples prepared, notwithstanding their varying intensity of the HT reflection and the larger size of the Ru^{3+} ions (0.068 nm) in comparison with the Al^{3+} ions (0.053 nm) [42]. This indicates that no substantial replacement of the Al^{3+} sites with Ru(III) ions took place and Ru existed in the amorphous phase separately from the HT [43]. For all catalysts calcined at 850 °C for 5 h, reflection lines of both Mg(Ni)-Al HT and $Mg(OH)_2$ brucite totally disappeared and replaced by those of Mg(Al,Ni)O periclase together with $Mg(Ni)Al_2O_4$ spinel.

Temperature gravimetric analyses (TGA) curves of three samples, 0.1 wt%Ru-$Ni_{0.5}/Mg_{2.5}$(Al)O (0.4, 1), 0.1 wt%Ru-$Ni_{0.5}/Mg_{2.5}$(Al)O (5, 1) and 0.1 wt%Ru-$Ni_{0.5}/Mg_{2.5}$(Al)O (40, 1) after the dipping, followed by drying, are shown in Fig. 7 a, b and c, respectively. All samples showed a weight loss up to 100 ºC due to the loss of physically adsorbed/interlayer water [44]. Between 100 and 230 ºC, weight was lost due to decarbonisation of the HT (DTA endotherm 225 ºC), followed by a further weight loss due to the dehydroxylation of the HT between 230 and 450 ºC (DTA endotherm 400 ºC) [43]. With increasing the amount of Ru(III) nitrate-aqueous solution, the weight loss of each step increased, indicating that the reconstitution of the HT was enhanced as previously observed in the XRD patterns (Fig. 6). Kloprogge and Frost [45] reported a similar change in the thermal transformation of Mg-Al HT using DT/TGA and infrared emission spectroscopy (IES). IES results show major changes around 350-450 ºC, suggesting the end of the dehydroxylation. 'Al'-OH bands

disappear in this temperature range and some new bands are observed, indicating the formation of spinel ($MgAl_2O_4$) together with Mg(Al)O periclase as the main component.

4.4. Effect of the HT reconstitution on the catalytic activity.

The results of propane oxidation by the temperature-cycled operation over the 0.1 wt%Ru-$Ni_{0.5}/Mg_{2.5}$(Al)O (0.4, 1), (4, 1), (40, 1) and (40, 12) catalysts are shown Fig. 8 together with those over the 0.1 wt%Ru/$Mg_{2.5}(Ni_{0.5})$-Al HT (5,1) and $Ni_{0.5}/Mg_{2.5}$(Al)O catalysts as controls. The sustainability of the catalyst was evaluated by comparing the propane conversion at the 1st step and that at the 2nd step both at 600 ºC. High activity as well as high sustainability was obtained over 0.1 wt%Ru-$Ni_{0.5}/Mg_{2.5}$(Al)O (40, 12), (40, 1) and (5, 1) catalysts, whereas both 0.1 wt%Ru-$Ni_{0.5}/Mg_{2.5}$(Al)O (0.4,1) and 0.1 wt%Ru-$Mg_{2.5}(Ni_{0.5})$-Al HT (5, 1) catalysts showed a significant deactivation. The deactivations of the latter two catalysts were more severe than that observed for the $Ni_{0.5}/Mg_{2.5}$(Al)O catalyst.

Coking was suppressed by the Ru loading, and coke amount substantially varied depending on the preparation technique (Table 3). Less coking over both 0.1 wt%Ru-$Ni_{0.5}/Mg_{2.5}$(Al)O (0.4, 1) and 0.1 wt%Ru-$Mg_{2.5}(Ni_{0.5})$-Al HT (5, 1) is probably due to the presence of Ru. The best results were obtained over the 0.1 wt%Ru-$Ni_{0.5}/Mg_{2.5}$(Al)O (5, 1) catalyst, showing the highest values in both activity and sustainability together with the low coking. An interaction between Ni and Ru can be estimated by the decrease in the reduction temperature of Ni in the TPR measurements (Table 3 and *vide infra*) [13]. Use of a relatively small amount of the solution, i.e., 5 ml,

was sufficient to decrease the Ni reduction temperature from 887 °C for the $Ni_{0.5}/Mg_{2.5}(Al)O$ catalyst to 840 °C for the 0.1 wt%Ru-$Ni_{0.5}/Mg_{2.5}(Al)O$ (5, 1) catalyst. Use of neither 40 ml of the solution nor 12 h of dipping time was not necessary for giving high activity as well as high sustainability to the catalyst (Fig. 8). Under such conditions, the reduction temperature of Ni was still high as 849 °C for the 0.1 wt%Ru-$Ni_{0.5}/Mg_{2.5}(Al)O$ (40, 12) although the reconstitution of HT was completed (Fig. 6f). The HT reconstitution gave rise to high dispersion of both Ni and Ru species leading to a strong interaction between Ni and Ru. However, the results obtained above suggest that a deep reconstitution of HT is not always necessary but the surface reconstitution of particles must be important for the active catalysts.

4.5. Ni-Ru bimetallic active species.

TPR profiles of the Ru-$Ni_{0.5}/Mg_{2.5}(Al)O$ catalysts with varying Ru loadings are shown in Fig. 9. In the absence of Ru, i.e. for the $Ni_{0.5}/Mg_{2.5}(Al)O$ catalyst, a single and intensive peak appeared at 895 ºC (Fig. 9a). This reduction peak shifted toward lower temperature by the Ru loading (Fig. 9b-e); the shift became more significant with increasing the Ru loading on the $Ni_{0.5}/Mg_{2.5}(Al)O$ catalyst and, additionally, a weak and broad peak appeared around 400 ºC for the 0.5 wt%Ru-$Ni_{0.5}/Mg_{2.5}(Al)O$ catalyst (Fig. 9e). The decrease in the reduction temperature of Ni suggests either a formation of RuNi alloy or an occurring of strong interaction between Ru and Ni. The weak and broad peak observed around 400 ºC for 0.5 wt%Ru-$Ni_{0.5}/Mg_{2.5}(Al)O$ catalyst can be ascribed to the reduction of RuO_2 to Ru metal, since no other stable ruthenium oxides are known to exist in the solid state [46,47]. This indicates that a part of Ru was

separated from Ru-Ni binary system. The TPR of Ru/Al_2O_3 and Ru/MgO catalysts showed the Ru reduction peak around 250 ºC and 235 ºC, respectively [48,49]. However, a strong metal-support interaction was frequently observed on the catalyst having well-dispersed Ru particles, causing an increase in the reduction temperature. It seems that, in contrast to TiO_2, Al_2O_3 has a tendency to stabilize ruthenium in the ionic state and the reduction temperature sometimes exceeds 700 ºC [49]. It is likely that the RuO_2 separated from Ru-Ni bimetallic system exist as fine particles, which were well dispersed on the catalyst surface and showed a reduction peak around 400 ºC in the TPR.

The 0.5 wt%Ru-$Ni_{0.5}/Mg_{2.5}$(Al)O catalyst showed a serious deactivation exceptionally at 400 ºC (Fig. 4A), however the activity was quickly recovered when the temperature was given back to 600 ºC. Balint et al. [47] reported that the equilibrium exists between RuO_2 and Ru metal around 450 ºC on 12 wt%Ru/Al_2O_3 catalyst in the partial oxidation of CH_4. The formation of RuO_2 phase in the reaction mixture (O_2/CH_4 = 1.87), which is favored in the temperature below 450 ºC, was found to be responsible for the combustion of CH_4 to CO_2 and H_2O. The $RuO_2 \leftrightarrow$ Ru equilibrium is shifted to the formation of Ru metal when the reaction temperature increased above 450 ºC. At the moment, the reaction rate increased considerably, and CO and H_2 simultaneously produced as the primary reaction products by the direct partial oxidation (6). Propane conversion decreased on the 0.5 wt%Ru-$Ni_{0.5}/Mg_{2.5}$(Al)O catalyst exceptionally at 400 ºC compared to those above 500 ºC (Fig. 4A). This phenomenon can be explained by the formation of RuO_2 at 400 ºC as observed in the TPR (Fig. 9e); Ru catalyzed direct partial oxidation of propane (4) above 500 ºC, whereas RuO_2 catalyzed the combustion

of propane (1) resulting in a decrease in propane conversion compared to the syngas formation by direct partial oxidation under the present molar ratio (1.87) of O_2/C_3H_8.

4.6. Role of Ru in the Ni-Ru bimetallic active species.

XRD patterns of both 0.1 and 0.5 wt%Ru-$Ni_{0.5}/Mg_{2.5}$(Al)O catalysts after the reduction are shown in Fig. 10 together with that of the $Ni_{0.5}/Mg_{2.5}$(Al)O catalyst as a control. The $Ni_{0.5}/Mg_{2.5}$(Al)O catalyst showed rather sharp and intensive reflection lines of Ni metal (Fig. 10Aa), which were broadened and shifted toward the lower reflection angles by the addition of 0.1 wt% Ru (Fig. 10Ab). Both line broadening and lower angle-shift became significant with increasing Ru loading up to 0.5 wt% (Fig. 10Ac) and were more clearly observed for the reflection of Ni (200) at 2 theta = 51.84° with increasing Ru loading (Fig. 10B a, b and c). It is suggested that RuNi alloy was formed and/or the size of Ni metal particles decreased still keeping the strong interaction with the support by the Ru loading on the Ru-$Ni_{0.5}/Mg_{2.5}$(Al)O catalysts.

Basile et al. [50] reported that Rh was completely soluble in the Mg(Al)O periclase phase, whereas Ru was not soluble in Mg(Al)O periclase and remained as separated phase, when both were incorporated into HT precursors with a large Mg/Al ratio. Such Ru species separated from the periclase reacted with Ni species liberated from $Mg_{2.5}$(Al,$Ni_{0.5}$)O periclase during the reduction, resulting in the formation of RuNi alloy and/or well dispersed Ni metal particles on the $Ni_{0.5}/Mg_{2.5}$(Al)O catalysts.

As shown in Table 2, H_2 uptake drastically enhanced by the Ru loading on the $Ni_{0.5}/Mg_{2.5}$(Al)O catalyst and increasing Ru loading resulted in a remarkable increase in the H_2 uptake. Particle sizes of Ni metal on the catalysts were calculated from the data

of both XRD and H_2 uptake (Table 2). In both cases, the Ni particle size on $Ni_{0.5}/Mg_{2.5}(Al)O$ was smaller than on *iw*-13.5wt%Ni/γ-Al_2O_3, and moreover decreased by the addition of noble metals on $Ni_{0.5}/Mg_{2.5}(Al)O$. This well coincided with the increase in the H_2 uptake by the addition of noble metals. With increasing the Ru loading, the Ni particle size decreased and the H_2 uptake increased. This can also be well explained by the dependency of the H_2 uptake on the metal particle size. The highest activity as well as the highest sustainability was obtained with the 0.1 wt%Ru-$Ni_{0.5}/Mg_{2.5}(Al)O$ (5, 1) catalyst. The contribution of Ru itself in the H_2 uptake on the Ru-$Ni_{0.5}/Mg_{2.5}(Al)O$ catalysts must be small, since the H_2 uptake was significantly small on the 0.1 wt%$Ru/Mg_3(Al)O$ catalyst. The reforming activity of the Ru-Ni bimetallic catalysts is mainly due to the presence of Ni metal on the catalysts surface, since the selectivity to H_2 was remarkably low on the 0.1 wt%$Ru/Mg_3(Al)O$ catalyst at 700 ºC (Table 1), although the conversions of both propane and oxygen were high enough on the 0.1 wt%$Ru/Mg_3(Al)O$ catalyst at 700 ºC (Fig. 4). It is likely that the catalytic property of Ni metal was enhanced by the Ru loading, probably due to an appearing of significant synergy between Ni and Ru metal by the bimetallic system formation. Ru quickly dissociates C-H bond to form H atoms which rapidly migrate to Ni surface by spillover, reduce the oxidized Ni and, as a result, keep the Ni species in the reduced and active state during the reaction.

5. Conclusion

Noble metals, i.e. Ru, Rh, Pd, Ir and Pt, and Ni bimetallic catalysts supported on Mg(Al)O periclase have been successfully applied for the partial oxidation of propane. Noble metals were supported on $Mg_{2.5}(Al,Ni_{0.5})O$ periclase derived from $Mg_{2.5}(Ni_{0.5})$-Al HT by adopting the "memory effect." The reconstitution of Mg(Ni)-Al HT took place on the surface of the $Mg_{2.5}(Al,Ni_{0.5})O$ periclase, where noble metals were included either by partly substituting Mg^{2+} or Al^{3+} sites in the HT or by being physically trapped in the layered structure, resulting in the highly dispersed noble metals-nickel bimetallic system. Among the noble metals tested, Ru was the most effective and 0.1 wt% of the loading afforded the highest activity as well as the highest sustainability in the temperature-cycled operation of propane partial oxidation. It seems that the catalyst deactivation took place due to the Ni oxidation either by gaseous oxygen or possibly by steam formed during the propane oxidation. It is concluded that Ru keeps the Ni surface in the reduced state by hydrogen atoms spilt over from Ru to Ni metals and showed the high and stable activity in the partial oxidation of propane.

References

1. M.A. Peña, J.P. Gómez, J.L.G. Fierro, Appl. Catal. A 144 (1996) 7.
2. J.N. Armor, Appl. Catal. A 176 (1999) 159.
3. J.R. Rostrup-Nielsen, Catal. Today 71 (2002) 243.
4. T. Shishido, M. Sukenobu, H. Morioka, R. Furukawa, H. Shirahase, K. Takehira, Catal. Lett. 73 (2001) 21.
5. T. Shishido, M. Sukenobu, H. Morioka, M. Kondo, Y. Wang, K. Takaki, K. Takehira, Appl. Catal. A 223 (2002) 35.
6. K. Takehira, T. Shishido, P. Wang, T. Kosaka, K. Takaki, Phys. Chem. Chem. Phys. 5 (2003) 3801.
7. K. Takehira, T. Shishido, P. Wang, T. Kosaka, K. Takaki, J. Catal. 221 (2004) 43.
8. K. Takehira, T. Shishido, D. Shouro, K. Murakami, M. Honda, T. Kawabata, K. Takaki, Appl. Catal. A 279 (2005) 41.
9. A.I. Tsyganok, M. Inaba, T. Tsunoda, K. Uchida, K. Suzuki, K. Takehira, T. Hayakawa, Appl. Catal. A 292 (2005) 328.
10. K. Takehira, T. Kawabata, T. Shishido, K. Murakami, T. Ohi, D. Shoro, M. Honda, K. Takaki, J. Catal. 231 (2005) 92.
11. T. Ohi, T. Miyata, D. Li, T. Shishido, T. Kawabata, T. Sano, K. Takehira, Appl. Catal. A 308 (2006) 194.
12. T. Miyata, D. Li, M. Shiraga, T. Shishido, Y. Oumi, T. Sano, K. Takehira, Appl. Catal. A 310 (2006) 97.

13. T. Miyata, M. Shiraga, D. Li, I. Atake, T. Shishido, Y. Oumi, T. Sano, K. Takehira, Catal. Commun. 8 (2007) 447.
14. F. Basile, G. Fornasari, F. Trifirò, A. Vaccari, Catal. Today 77 (2002) 215.
15. K. Nagaoka, A. Jentys, J.A. Lercher, J. Catal. 229 (2005) 185.
16. M. Nurunnabi, B. Li, K. Kunimori, K. Suzuki, K. Fujimoto, K. Tomishige, Appl. Catal. A 292 (2005) 272.
17. M. Nurunnabi, K. Fujimoto, K. Suzuki, B. Li, S. Kado, K. Kunimori, K. Tomishige, Catal. Commun. 7 (2006) 73.
18. M. Nurunnabi, Y. Mukainakano, S. Kado, B. Li, K. Kunimori, K. Suzuki, K. Fujimoto, K. Tomishige, Appl. Catal. A 299 (2006) 145.
19. J.A.C. Dias, J.M. Assaf, J. Power Sources, 130 (2004) 106.
20. J.A.C. Dias, J.M. Assaf, J. Power Sources, 139 (2005) 176.
21. J.H. Jeong, J.W. Lee, D.J. Seo, Y. Seo, W.L. Yoon, D.K. Lee, D.H. Kim, Appl. Catal. A 302 (2006) 151.
22. D.A. Goetsch, L.D. Schmidt, Science 271 (1996) 1560.
23. A.S. Bodke, S.S. Bharadwaj, L.D. Schmidt, J. Catal. 179 (1998) 138.
24. S. Ayabe, H. Omoto, T. Utaka, R. Kikuchi, K. Sasaki, Y. Teraoka, K. Eguchi, Appl. Catal. A 241 (2003) 261.
25. I. Aartun, T. Gjervan, H. Venvik, O. Görke, P. Pfeifer, M. Fathi, A. Holmen, K. Schubert, Chem. Eng. J. 101 (2004) 93.
26. B. Silberova, H.J. Venvik, A. Holmen, Catal. Today 99 (2005) 69.
27. S. Liu, L. Xu, S. Xie, Q. Wang, G. Xiong, Appl. Catal. A 211 (2001) 145.

28. K. Schulze, W. Makowski, R. Chyży, R. Dziembaj, G. Geismar, Appl. Clay Sci. 18 (2001) 59.

29. A.K. Avci, D.L. Trimm, A.E. Aksoylu, Z.İ. Önsan, Catal. Lett. 88 (2003) 17.

30. A.K. Avci, D.L. Trimm, A.E. Aksoylu, Z.İ. Önsan, Appl. Catal. A 258 (2004) 235.

31. B.S. Çağlayan, A.K. Avci, Z.İ. Önsan, A.E. Aksoylu, Appl. Catal. A 280 (2005) 181.

32. C.H. Bartholomew, R.B. Pannell, J.L. Butler, J. Catal. 65 (1980) 335.

33. S. Wang, H.Y. Zhu, G.Q. Lu, J. Colloid Interface Sci. 204 (1998) 128.

34. V.A. Tsipouriari, Z. Zhang, X.E. Verykios, J. Catal. 179 (1998) 283.

35. H.S. Bengaard, J.K. Nørskov, J. Sehested, B.S. Clausen, L.P. Nielsen, A.M. Molenbroek, J.R. Rostrup-Nielsen, J. Catal. 209 (2002) 365.

36. S. Natesakhawat, R.B. Watson, X. Wang, U.S. Ozkan, J. Catal. 234 (2005) 496.

37. J.W. Shabaker, G.W. Huber, J.A. Dumesic, J. Catal. 222 (2004) 180.

38. J.W. Shabaker, D.A. Simonetti, R.D. Cortright, J.A. Dumesic, J. Catal. 231 (2005) 67.F.

39. T. Sperle, D. Chen, R. Lødeng, A. Holmen, Appl. Catal. A 282 (2005) 195.

40. J.R. Rostrup-Nielsen, in “Catalysis, Science and Technology” J.R. Anderson and M. Boudart, Eds. Vol. 5, p. 1. Sppringer-Verlag, Berlin/New York, 1984.

41. J.H. Eun, J.H. Lee, S.G. Kim, M.Y. Um, S.Y. Park, H.J. Kim, Thin Solid Films 435 (2003) 199.

42. R.D. Shannon, Acta Crystallogr. A 32 (1976) 751.

43. F. Basile, G. Fornasari, M. Gazzano, A. Vaccari, Appl. Clay Sci. 16 (2000) 185.

44. F. Cavani, F. Trifirò, A. Vaccari, Catal. Today 11 (1991) 173.

45. J.T. Kloprogge, R.L. Frost, Appl. Catal. A 184 (1999) 61.

46. H. Madhavaram, H. Idriss, S. Wendt, Y.D. Kim, M. Knapp, H. Over, J. Aβmann, E. Löffler, M. Muhler, J. Catal. 202 (2001) 296.

47. I. Balint, A. Miyazaki, K. Aika, J. Catal. 220 (2003) 74.

48. S.-F. Yin, Q.-H. Zhang, B.-Q. Xu, W.-X. Zhu, C.-F. Ng, C.-T. Au, J. Catal. 224 (2004) 384.

49. C. Elmasides, D.I. Kondarides, W. Grünert, X.E. Verykios, J. Phys. Chem. B 103 (1999) 99.

50. F. Basile, G. Fornasari, V. Rosetti, F. Trifirò, A. Vaccari, Catal. Today 91-91 (2004) 293.

Table 1. Product distribution in partial oxidation of propane[a)]

Catalyst[b)]	Selectivity to H_2 / %	Selectivity / %						Coke deposition / wt%[c)]
		CO	CO_2	CH_4	C_2H_4	C_2H_6	C_3H_6	
$Ni_{0.5}/Mg_{2.5}(Al)O$	78.4	76.8	15.0	4.6	3.2	0.4	0.0	40.4
iw-13.5wt%Ni/γ-Al_2O_3	83.4	78.2	15.7	4.1	1.6	0.2	0.2	80.0
0.1wt%Ru/$Mg_3(Al)O$[d)]	39.7	59.9	11.6	11.4	13.6	2.0	1.5	1.8
0.1wt%Ru-$Ni_{0.5}/Mg_{2.5}(Al)O$	84.9	81.7	14.1	4.2	0.0	0.0	0.0	6.1
0.1wt%Rh-$Ni_{0.5}/Mg_{2.5}(Al)O$	85.8	81.0	14.6	4.3	0.1	0.0	0.0	18.9
0.1wt%Pd-$Ni_{0.5}/Mg_{2.5}(Al)O$	82.8	80.4	14.0	4.8	0.7	0.1	0.0	13.1
0.1wt%Ir-$Ni_{0.5}/Mg_{2.5}(Al)O$	76.6	74.8	13.7	5.2	5.1	0.6	0.6	11.5
0.1wt%Pt-$Ni_{0.5}/Mg_{2.5}(Al)O$	84.0	81.0	13.8	4.7	0.5	0.1	0.0	24.8
0.5wt%Ru-$Ni_{0.5}/Mg_{2.5}(Al)O$	86.4	81.4	14.5	4.1	0.0	0.0	0.0	4.4
0.05wt%Ru-$Ni_{0.5}/Mg_{2.5}(Al)O$	85.7	81.2	14.5	4.3	0.0	0.0	0.0	21.0
0.01wt%Ru-$Ni_{0.5}/Mg_{2.5}(Al)O$	82.9	79.8	14.6	4.5	1.0	0.1	0.0	63.9
0.1wt%Ru-$Ni_{0.5}/Mg_{2.5}(Al)O(0.4)$[e)]	84.0	81.2	13.7	4.5	0.5	0.1	0.0	5.0
0.1wt%Ru-$Ni_{0.5}/Mg_{2.5}(Al)O(40)$[f)]	85.7	81.2	14.0	4.7	0.1	0.0	0.0	14.6
0.1wt%Ru-$Ni_{0.5}/Mg_{2.5}(Al)O_{HTlc}$[g)]	82.2	78.1	13.7	4.8	2.7	0.4	0.3	3.1
FCR[h)]	69.3	71.2	23.7	1.4	1.3	0.1	2.3	11.8
RUA[i)]	47.0	64.1	12.8	9.9	10.0	1.7	1.5	0.4

a) Reaction temperature, 700 ºC; propane conversion, 100 % ([d)] 99.2 %, [h)] 78.3 %, [i)] 98.8 %).

b) Metal loading was carried out by dipping 1.0 g of the powder of $Ni_{0.5}/Mg_{2.5}(Al)O$ in 5 ml (0.4 ml[e)] and 40 ml[f)]) of aqueous solution of the nitrates of noble metals for 1 h at room temperature.

c) Obtained by TPO experiment for the catalysts after the reaction.

g) One gram of the powder of $Mg_{2.5}(Al,Ni_{0.5})$-HT after drying was used.

Table 2. Physicochemical properties of noble metal-Ni supported catalysts.

Catalyst[a]	BET surface area[b] / $m^2\ g_{cat}^{-1}$	H_2 uptake[c] / $\mu mol\ g_{cat}^{-1}$	Dispersion[d] / %	Particle size of Ni metal / nm	
				XRD[e]	H_2 up take[d]
$Ni_{0.5}/Mg_{2.5}(Al)O$	158.0	120.7	13.1	6.9	7.4
iw-13.5wt%Ni/γ-Al_2O_3	106.3	74.4	6.5	10.0	14.9[f]
0.1wt%Ru/$Mg_3(Al)O$	121.5	0.56	-	-	-
0.1wt%Ru-$Ni_{0.5}/Mg_{2.5}(Al)O$	146.7	221.9	24.0	5.2	4.0
0.1wt%Rh-$Ni_{0.5}/Mg_{2.5}(Al)O$	148.4	184.0	19.9	5.7	4.9
0.1wt%Pd-$Ni_{0.5}/Mg_{2.5}(Al)O$	134.9	148.8	16.1	5.8	6.0
0.1wt%Ir-$Ni_{0.5}/Mg_{2.5}(Al)O$	140.0	204.2	22.1	5.3	4.4
0.1wt%Pt-$Ni_{0.5}/Mg_{2.5}(Al)O$	134.9	225.3	24.4	5.5	4.0
0.5wt%Ru-$Ni_{0.5}/Mg_{2.5}(Al)O$	148.0	261.4	28.3	5.0	3.4
0.05wt%Ru-$Ni_{0.5}/Mg_{2.5}(Al)O$	138.3	187.2	20.3	5.7	4.8
0.01wt%Ru-$Ni_{0.5}/Mg_{2.5}(Al)O$	137.7	183.5	19.9	5.7	4.9
0.1wt%Ru-$Ni_{0.5}/Mg_{2.5}(Al)O_{0.4\ ml}$[g]	118.4	-	-	-	-
0.1wt%Ru-$Ni_{0.5}/Mg_{2.5}(Al)O_{40\ ml}$[h]	140.2	-	-	-	-
0.1wt%Ru-$Ni_{0.5}/Mg_{2.5}(Al)O_{HTlc}$[i]	154.1	-	-	-	-
FCR	7.0	-	-	-	-
RUA	6.5	-	-	-	-

a) Metal loading was carried out by dipping 1.0 g of the powder of $Ni_{0.5}/Mg_{2.5}(Al)O$ in 5 ml (0.4 ml[g] and 40 ml[h]) of aqueous solution of the nitrates of noble metals for 1 h at room temperature.

b) Calcined at 850 ºC for 5 h.

c) Determined by the H_2 pulse method.

d) Calculated from the H_2 uptake assuming the reduction degree of 80 % for hydrotalcite derived catalyst [13] and 100 % for impregnated catalyst. [f]

e) Calculated from the full width at half maximum of the reflection of Ni (200) plane in the XRD using Scherrer equation.

i) One gram of the powder of $Mg_{2.5}(Ni_{0.5})$-Al HT was used.

Table 3. Preparation method of Ru-$Ni_{0.5}/Mg_{2.5}$(Al)O catalysts and their some properties.

Catalyst[a)]	Amount of $Ru(NO_3)_3$ aqueous solution / ml	Dipping time / h	Support form[b)]	Drying method	Coke formed[c)] / %	Ni reduction temperature[d)] / °C
$Ni_{0.5}/Mg_{2.5}$(Al)O					40.4	887
0.1 wt%Ru-$Ni_{0.5}/Mg_{2.5}$(Al)O (0.4, 1)	0.4	1	powder	105 °C, one night	5.0	845
0.1 wt%Ru-$Ni_{0.5}/Mg_{2.5}$(Al)O (5, 1)	5	1	powder	75 °C, 0.5 h + 105 °C, one night	6.1	840
0.1 wt%Ru-$Ni_{0.5}/Mg_{2.5}$(Al)O (40, 1)	40	1	powder	90 °C, 3 h + 105 °C, one night	14.6	852
0.1wt%Ru-$Ni_{0.5}/Mg_{2.5}$(Al)O (40, 12)	40	12	powder	90 °C, 3 h + 105 °C, one night	-	849
0.1 wt%Ru/$Mg_{2.5}(Ni_{0.5})$-Al HT (5, 1)[e)]	5	1	powder	75 °C, 0.5 h + 105 °C, one night	3.1	-
0.1wt%Ru/Mg_3(Al)O (5, 1)	5	1	powder	75 °C, 0.5 h + 105 °C, one night	1.8	-

[a)] Metal loading was carried out by dipping 1.0 g of the powder of $Ni_{0.5}/Mg_{2.5}$(Al)O or $Mg_{2.5}(Ni_{0.5})$-Al HT[e)] in 0.4, 5 or 40 ml of aqueous solution of Ru(III) nitrate for 1 or 12 h at room temperature.

[b)] Powder: obtained by finely crushing with agate mortar.

[c)] Obtained by TPO of the catalysts after the temperature-cycled oxidation.

[d)] Obtained by TPR of the catalysts.

Figure captions

Fig. 1 Temperature-cycled operation mode for the partial oxidation of propane.

Fig. 2 XRD patterns of the 0.1 wt%Ru-$Ni_{0.5}/Mg_{2.5}$(Al)O catalyst during the preparation. a) $Mg_{2.5}(Ni_{0.5})$Al-HT after the co-precipitation; b) $Mg_{2.5}$(Al,$Ni_{0.5}$)O periclase after the calcination; c) 0.1 wt%Ru-$Mg_{2.5}$(Al,$Ni_{0.5}$)O after the dipping; d) 0.1 wt%Ru-$Ni_{0.5}/Mg_{2.5}$(Al)O after the calcination; e) 0.1 wt%Ru-$Ni_{0.5}/Mg_{2.5}$(Al)O after the reduction; f) 0.1 wt%Ru-$Ni_{0.5}/Mg_{2.5}$(Al)O after the reaction.

○, $Mg_{2.5}(Ni_{0.5})$Al-HT; ●, $Mg_{2.5}$(Al,$Ni_{0.5}$)O periclase; ▲, Ni metal; ■, $Mg(Ni)_2Al_2O_4$ spinel.

Fig. 3 Partial oxidation of propane by temperature-cycled operation over noble metal-supported catalysts.

A: Propane conversion; B: Selectivity to H_2O.

○, 0.1 wt%Ru-$Ni_{0.5}/Mg_{2.5}$(Al)O; □, 0.1 wt%Rh-$Ni_{0.5}/Mg_{2.5}$(Al)O; Δ, 0.1 wt%Pd-$Ni_{0.5}/Mg_{2.5}$(Al)O; ■, 0.1 wt%Ir-$Ni_{0.5}/Mg_{2.5}$(Al)O; ●, 0.1 wt%Pt-$Ni_{0.5}/Mg_{2.5}$(Al)O; ▲, $Ni_{0.5}/Mg_{2.5}$(Al)O; ×, imp-Ni/γ-Al_2O_3; +, FCR; ∗, RUA.

Fig. 4 Partial oxidation of propane by temperature-cycled operation over Ru-supported catalysts.

A: Propane conversion; B: Selectivity to H_2O.

■, 0.5 wt%Ru-$Ni_{0.5}/Mg_{2.5}$(Al)O; ○, 0.1 wt%Ru-$Ni_{0.5}/Mg_{2.5}$(Al)O; ●, 0.05 wt%Ru-$Ni_{0.5}/Mg_{2.5}$(Al)O; □, 0.01 wt%Ru-$Ni_{0.5}/Mg_{2.5}$(Al)O; ▲,

$Ni_{0.5}/Mg_{2.5}(Al)O$; Δ, 0.1 wt%Ru/$Mg_3(Al)O$.

Fig. 5 Temperature programmed oxidation of the supported Ru catalysts after the reaction.

a) 0.1 wt%Ru/$Mg_3(Al)O$; b) $Ni_{0.5}/Mg_{2.5}(Al)O$; c) 0.01 wt%Ru-$Ni_{0.5}/Mg_{2.5}(Al)O$; d) 0.05 wt%Ru-$Ni_{0.5}/Mg_{2.5}(Al)O$; e) 0.1 wt%Ru-$Ni_{0.5}/Mg_{2.5}(Al)O$; f) 0.5 wt%Ru-$Ni_{0.5}/Mg_{2.5}(Al)O$.

Fig. 6 XRD patterns of the samples of 0.1 wt%Ru-$Ni_{0.5}/Mg_{2.5}(Al)O$ after the dipping in varying volume of Ru(III) nitrate-aqueous solution.

a) $Mg_{2.5}(Ni_{0.5})$Al-HT as prepared; b) $Mg_{2.5}(Al,Ni_{0.5})O$ periclase after calcination; c) 0.1 wt%Ru-$Ni_{0.5}/Mg_{2.5}(Al)O$ (0.4, 1); d) 0.1 wt%Ru-$Ni_{0.5}/Mg_{2.5}(Al)O$ (5, 1); e) 0.1 wt%Ru-$Ni_{0.5}/Mg_{2.5}(Al)O$ (40, 1); f) 0.1 wt%Ru-$Ni_{0.5}/Mg_{2.5}(Al)O$ (40, 12); g) 0.1 wt%Ru-$Mg_{2.5}(Ni_{0.5})$Al-HT.

○, $Mg_{2.5}(Ni_{0.5})$Al-HT; ●, $Mg_{2.5}(Al,Ni_{0.5})O$ periclase; □. $Mg(OH)_2$ brucite.

Fig. 7 TGA curves of the samples of 0.1 wt%Ru-$Ni_{0.5}/Mg_{2.5}(Al)O$ after the dipping in varying volume of Ru(III) nitrate-aqueous solution.

a) 0.1 wt%Ru-$Ni_{0.5}/Mg_{2.5}(Al)O$ (0.4); b) 0.1 wt%Ru-$Ni_{0.5}/Mg_{2.5}(Al)O$ (5.0); c) 0.1 wt%Ru-$Ni_{0.5}/Mg_{2.5}(Al)O$ (40).

Fig. 8 Sustainability of the Ru-$Ni_{0.5}/Mg_{2.5}(Al)O$ catalysts during the temperature-cycled oxidation of propane.

1^{st}: the propane conversion obtained by the 1^{st} operation at 600 ºC; 2^{nd}: the propane conversion obtained by the 2^{nd} operation at 600 ºC.

Fig. 9 Temperature programmed reduction of supported Ru catalysts.

a) $Ni_{0.5}/Mg_{2.5}(Al)O$; b) 0.01 wt%Ru-$Ni_{0.5}/Mg_{2.5}(Al)O$; c) 0.05

wt%Ru-$Ni_{0.5}/Mg_{2.5}$(Al)O; d) 0.1wt %Ru-$Ni_{0.5}/Mg_{2.5}$(Al)O; e) 0.5 wt%Ru-$Ni_{0.5}/Mg_{2.5}$(Al)O.

Fig. 10 XRD patterns of the supported Ru-Ni bimetallic catalysts after the reduction.

a) $Ni_{0.5}/Mg_{2.5}$(Al)O; b) 0.1 wt%Ru-$Ni_{0.5}/Mg_{2.5}$(Al)O; c) 0.5 wt%Ru-$Ni_{0.5}/Mg_{2.5}$(Al)O.

●, $Mg_{2.5}(Al,Ni_{0.5})O$ periclase; ▲, Ni metal; ■, $Mg(Ni)_2Al_2O_4$ spinel.

Figure 1. K. Takehira et al.

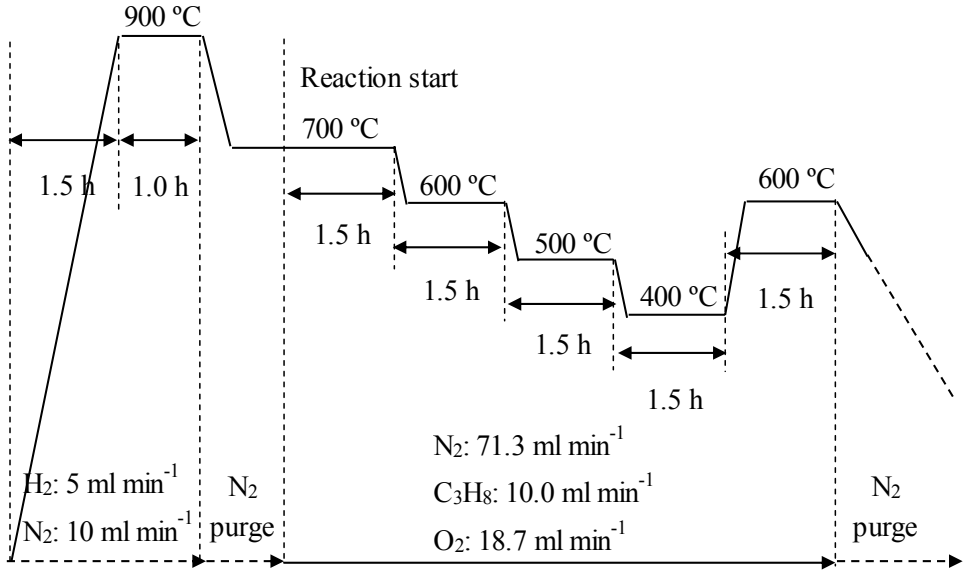

Figure 2. K. Takehira et al.

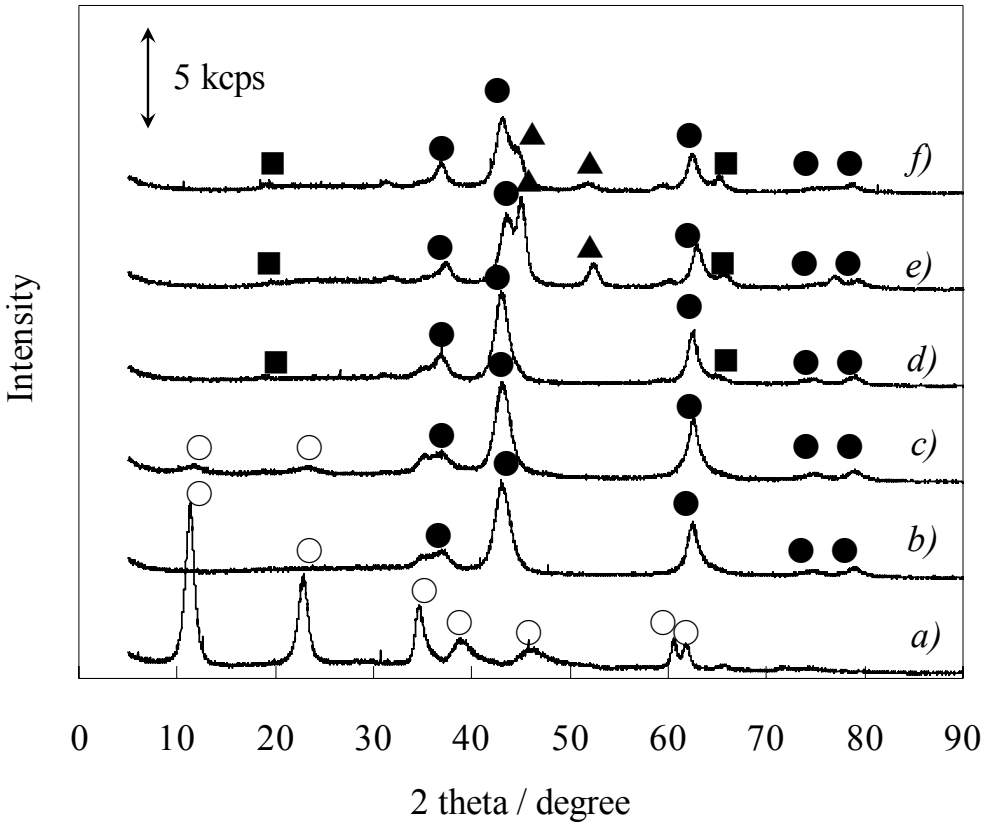

Figure 3. K. Takehira et al.

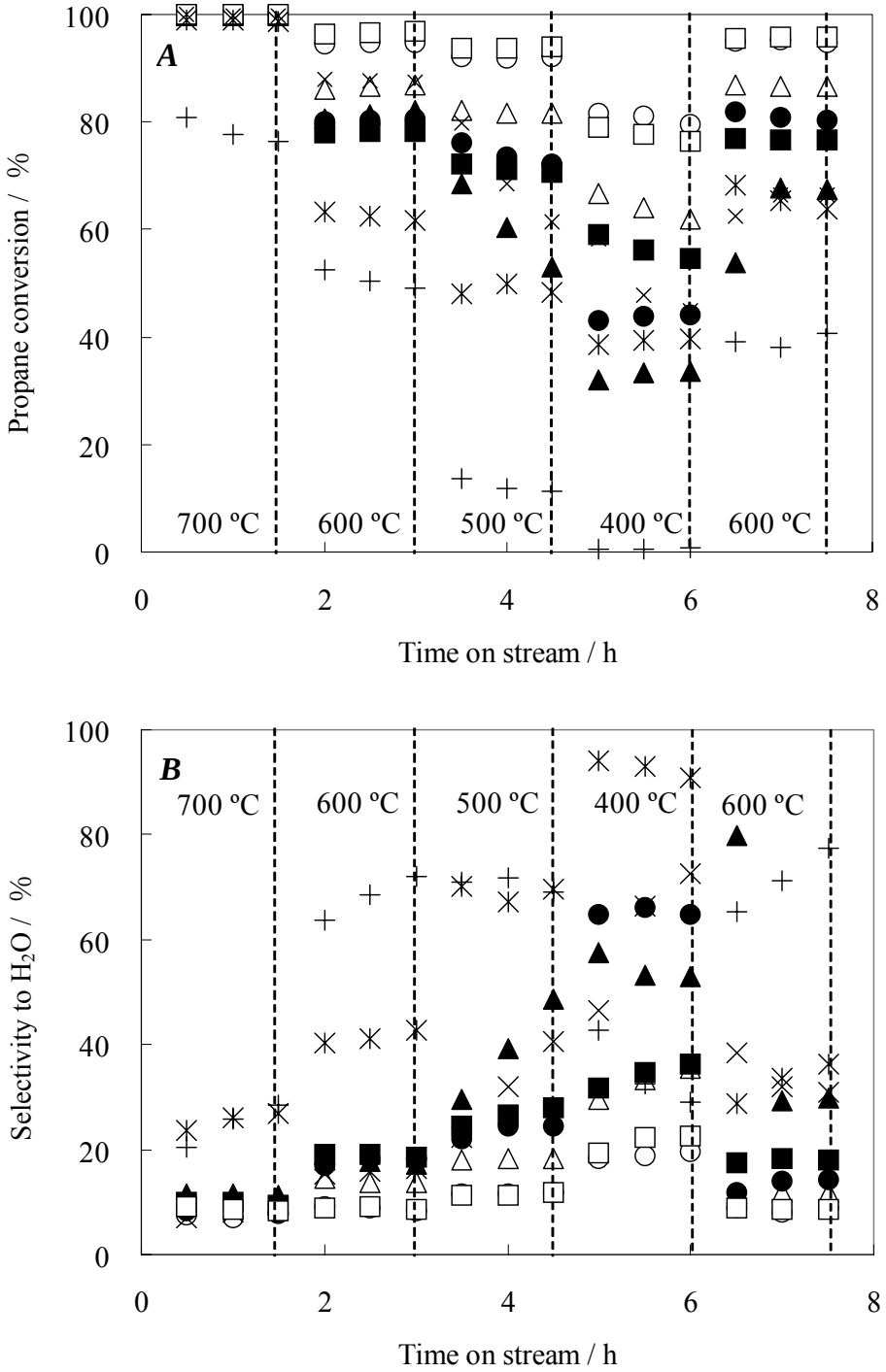

Figure 4. K. Takehira et al.

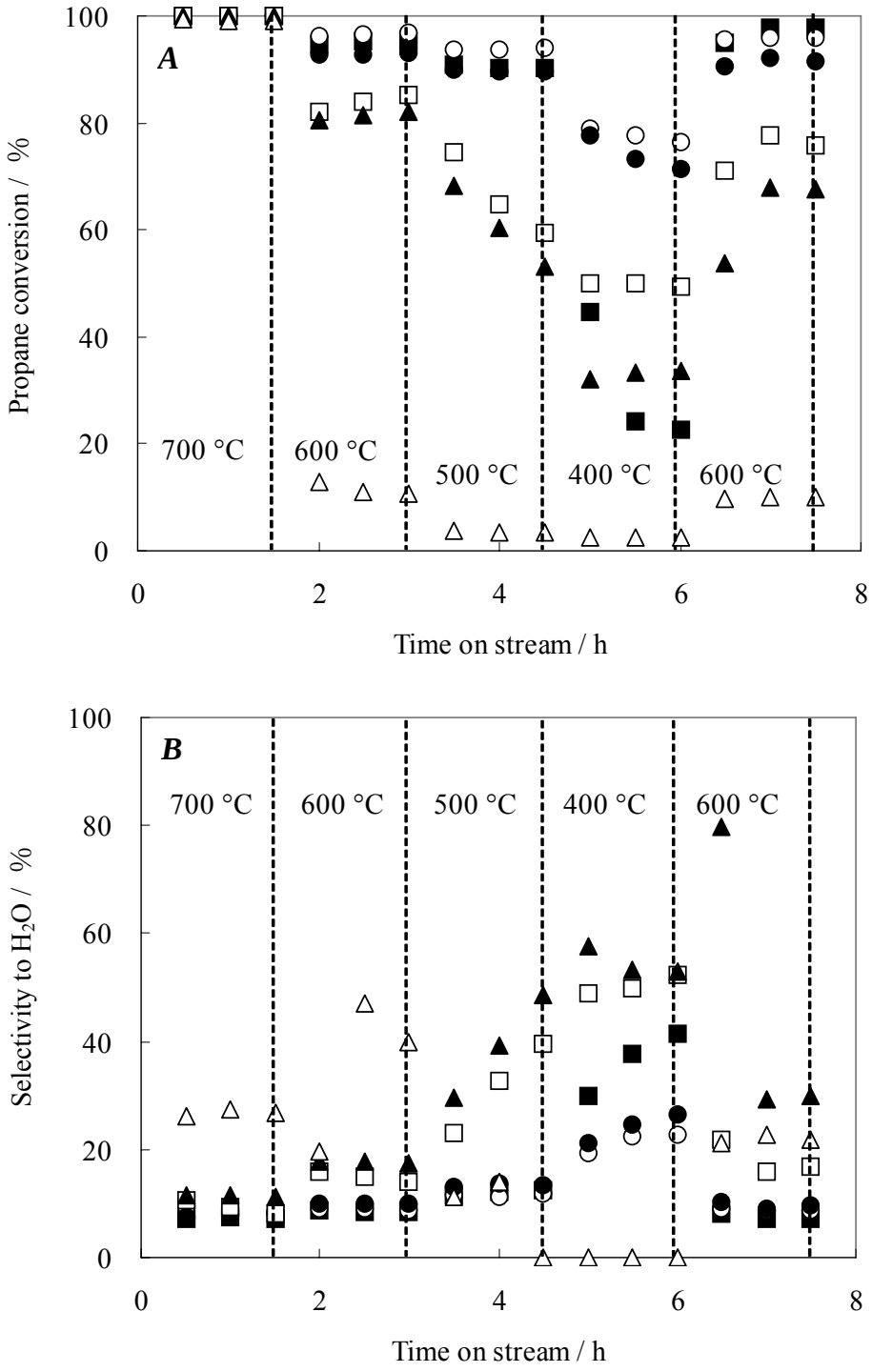

Figure 5. K. Takehira et al.

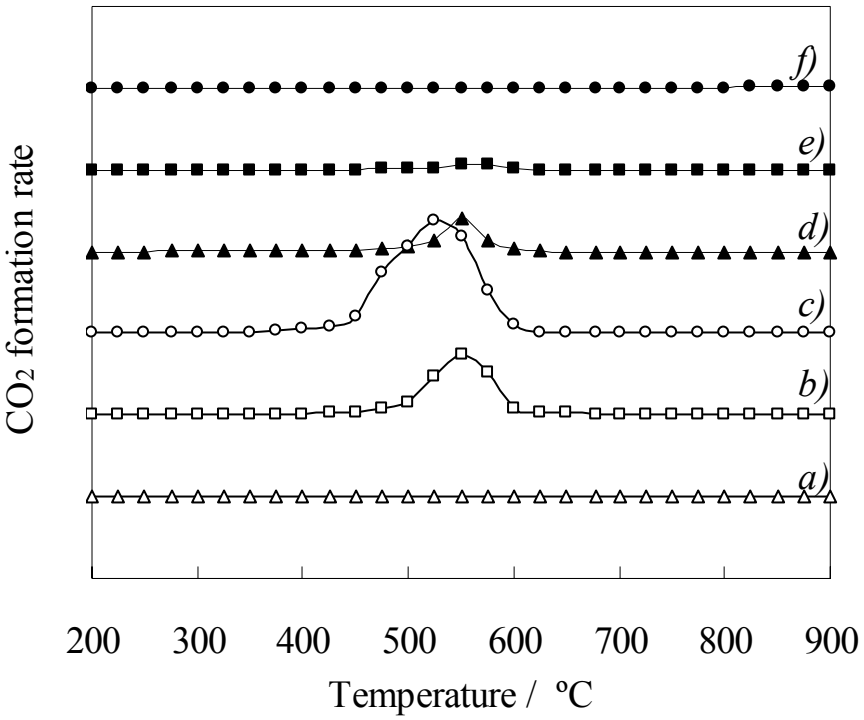

Figure 6. K. Takehira et al.

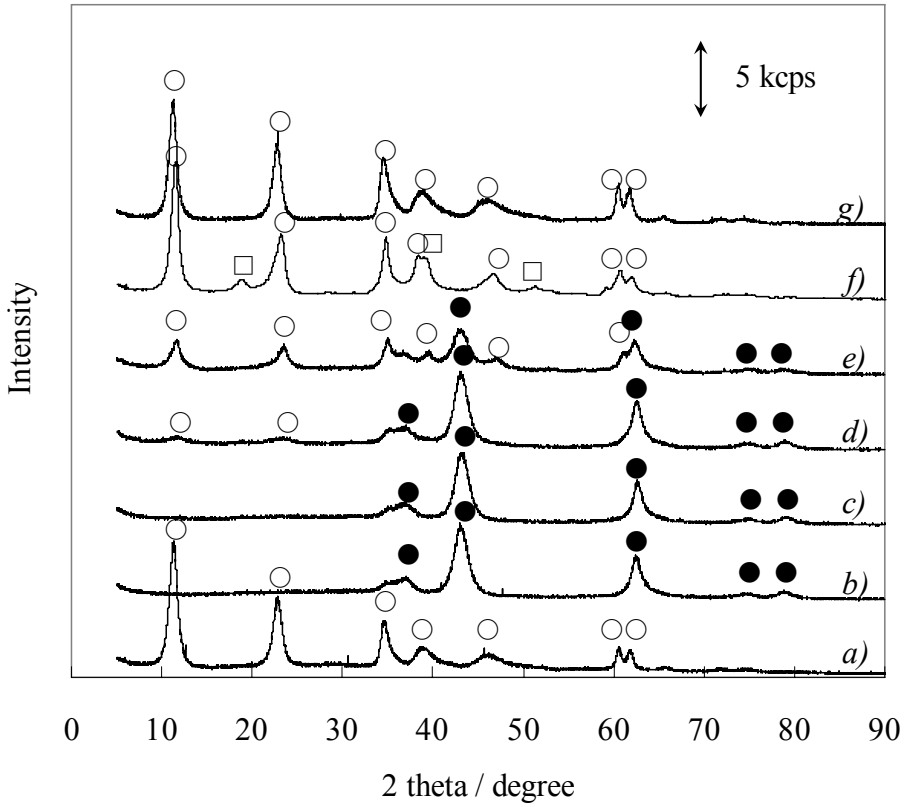

Figure 7. K. Takehira et al.

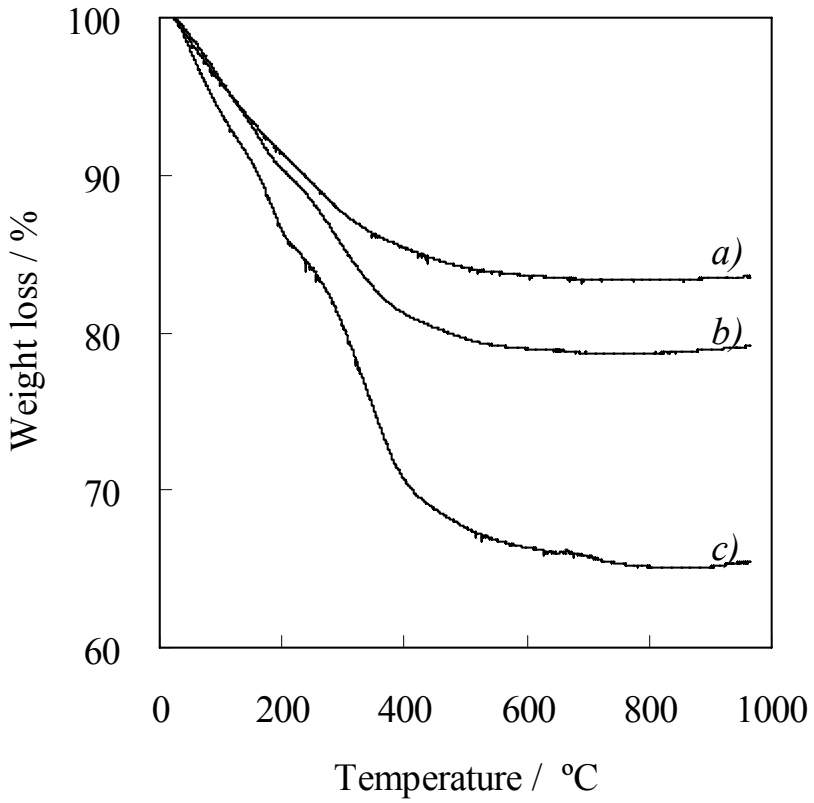

Figure 8. K. Takehira et al.

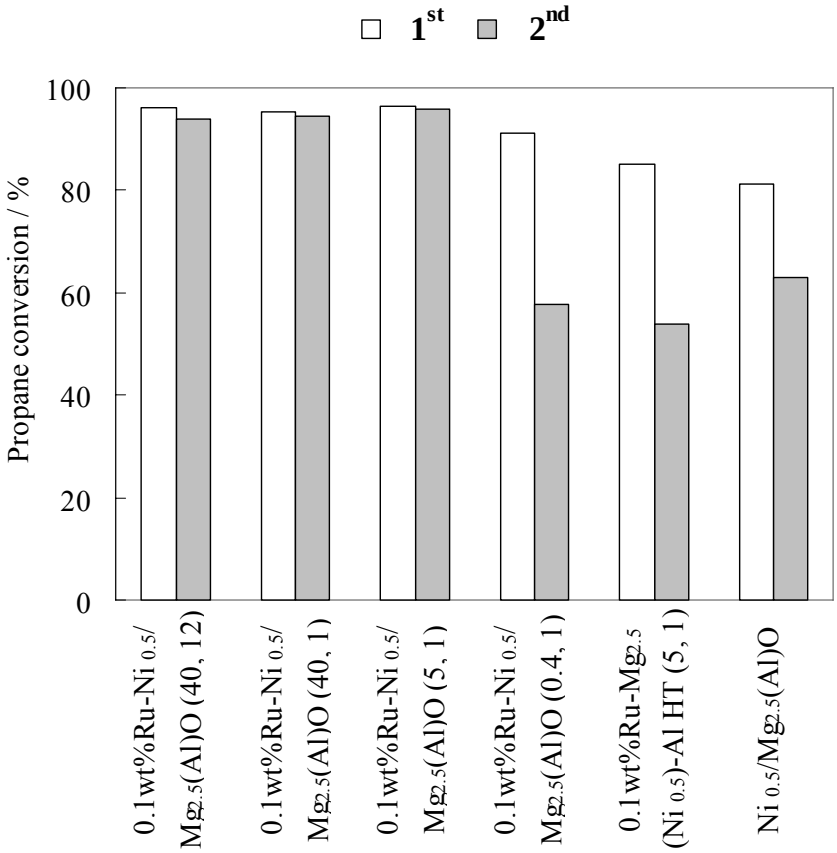

Figure 9. K. Takehira et al.

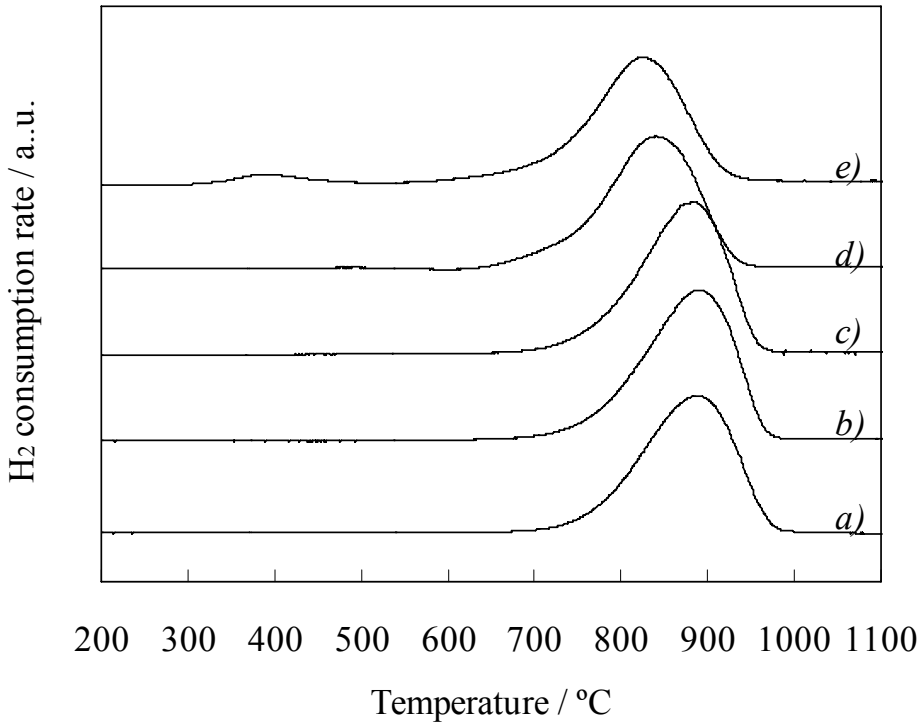

Figure 10. K. Takehira et al